Quantitative second-harmonic generation microscopy in collagen

Patrick Stoller, Peter M. Celliers, Karen M. Reiser, and Alexander M. Rubenchik

The second-harmonic signal in collagen, even in highly organized samples such as rat tail tendon fascicles, varies significantly with position. Previous studies suggest that this variability may be due to the parallel and antiparallel orientation of neighboring collagen fibrils. We applied high-resolution second-harmonic generation microscopy to confirm this hypothesis. Studies in which the focal spot diameter was varied from ~1 to ~6 μm strongly suggest that regions in which collagen fibrils have the same orientation in rat tail tendon are likely to be less than ~1 μm in diameter. These measurements required accurate determination of the focal spot size achieved by use of different microscope objectives; we developed a technique that uses second-harmonic generation in a quartz reference to measure the focal spot diameter directly. We also used the quartz reference to determine a lower limit ($d_{XXX} > 0.4$ pm/V) for the magnitude of the second-order nonlinear susceptibility in collagen.

OCIS codes: 190.1900, 190.4710, 180.5810, 170.5810, 170.0180, 170.7160.

1. Introduction

Several recent studies have taken advantage of Ti: sapphire mode-locked lasers—reliable, tunable, low-maintenance sources of ~100-fs pulses in the near infrared—to investigate second-harmonic generation (SHG) in biological tissue.[1–13] SHG is a coherent process in which two photons at the fundamental frequency are converted into a single photon at twice the frequency without absorption and reemission; this process can occur only in materials that lack a center of inversion symmetry and that are organized on the scale of the wavelength of the laser light. Fibrillar collagen—particularly its most abundant form, type I collagen—is one of the major constituents of tissue that are responsible for SHG.[2,7,13–15] Inasmuch as changes in collagen structure are important in many pathological conditions—ranging from diabetes to skin cancer—SHG microscopy presents an important potential diagnostic tool.

In previous studies[10,11] a high degree of variability was observed in the strength of the second-harmonic signal in two-dimensional scans of collagenous tissues, even in structurally homogeneous tissues such as rat tail tendon. Previous reports by investigators who used SHG and sum-frequency generation suggest that parallel and antiparallel orientation of neighboring collagen fibrils may be responsible for this variability.[16–18] However, Freund *et al.*[18] concluded from these results that collagen may not be responsible for SHG in rat tail tendon. Because other experiments[2,7,13–15] have demonstrated conclusively that collagen is responsible for SHG, the conclusions of Freund *et al.* suggest that further study is required. In the present study we investigate the hypothesis that the degree of parallel and antiparallel orientation of neighboring fibrils is responsible for the large variation in second-harmonic signal. Using objectives with different numerical apertures, we have obtained information on a microscopic scale (~1- to ~6-μm resolution). We present a technique that uses SHG in a quartz plate to measure properties of the focal spot; this technique allows us to compare measurements made with different objectives. Use of the quartz plate as a reference has the added advantages of allowing us to measure the absolute power generated in a collagen sample as a function of position and to place a lower limit on the second-order nonlinear susceptibility of rat tail tendon collagen.

P. Stoller and P. M. Celliers (celliers1@llnl.gov) are with M Division, Lawrence Livermore National Laboratory, L-174, P.O. Box 808, Livermore, California 94551. K. M. Reiser is with the Department of Neurological Surgery, School of Medicine, University of California, Davis, Room 0202, 2315 Stockton Boulevard, Sacramento, California 95817. A. M. Rubenchik is with the NIF Program, Lawrence Livermore National Laboratory, L-399, P.O. Box 808, Livermore, California 94551.

Received 10 September 2002; revised manuscript received 6 January 2003.

0003-6935/03/255209-11$15.00/0

Table 1. Microscope Objectives Used in the Experiment

Nominal Magnification	Manufacturer/Type	N.A.	Working Distance (mm)
10×	Mitutoyo/plano–apochromat	0.28	33.5
20×	Mitutoyo/plano–apochromat	0.42	20.0
40×	Nikon/s fluor	0.90	0.3

2. Experiment

A. Optical Setup

We used a Ti:sapphire oscillator (Mira; Coherent, Inc., Santa Clara, Calif.) to generate linearly polarized ~200-fs pulses at a wavelength of 800 nm with a maximum energy of 5 nJ and at a repetition rate of 76 MHz. A Faraday isolator was used to prevent backscattered light from entering the laser cavity and interfering with mode locking. The beam passed through a half-wave plate followed by a polarizing beam splitter; we rotated the half-wave plate to control the power incident upon the sample. The *p*-polarized light transmitted through the beam splitter was chopped at 1.5 kHz by an optical chopper and then passed through an electro-optic modulator (360-80; Conoptics, Danbury, Conn.) with its axes oriented at 45 deg to the polarization of the light. The beam was passed through a spatial filter and beam expander (a 50-mm lens focused the beam onto a 50-μm pinhole). The beam then passed through a quarter-wave plate with its axes oriented at 45 deg to those of the electro-optic modulator (EOM). We used the EOM–quarter-wave plate combination to rotate the polarization direction of the linearly polarized laser light; rotating the polarization of the light continuously ensures that the second-harmonic signal is independent of the orientation of collagen fibrils in the sample (a more detailed description is provided in a previous paper[11]).

Several microscope objectives (refer to Table 1) were used to focus the beam onto a sample mounted on an *x*–*y*–*z*, computer-controlled translation stage; we refer to the objects as the 10×, 20×, and 40× objectives. We used these different microscope objectives combined with collimating lenses of different focal lengths in the beam expander (50, 100, and 200 mm) to obtain different numerical apertures for focusing the beam. An iris was used to allow only the central maximum of the Airy pattern produced by the spatial filter to enter the back aperture of the microscope objectives. A laser powermeter was inserted into the beam path to measure the average power of the laser beam; we determined that the fractional transmission of all three objectives was the same to within the uncertainty of the power measurement. Thus the same power was incident upon the sample for all combinations of collimating lenses and microscope objectives used.

The transmitted second-harmonic signal was collected with a Mitutoyo 100× (N.A., 0.7; working distance, 6.0 mm) objective; other objectives did not have a suitably long working distance for use in our setup. Some undercollection of the SHG signal generated by the 40× objective (N.A., 0.9) occurred. An interference filter was used to reject the first harmonic and to allow only the second-harmonic signal to reach the photomultiplier tube (H6780; Hamamatsu Photonics K.K., Hamamatsu City, Japan). A fiber lamp (used while there was no scanning to illuminate the sample through the collecting objective), a pellicle-beam splitter (flipped into the beam path before the microscope objective when there was no scanning), a lens, and a CCD camera were used to image the sample and the focal spot of the laser. The experimental setup is illustrated in Fig. 1.

After passing through a current preamplifier (SR570; Stanford Research Systems, Sunnyvale, Calif.), the signal from the photomultiplier tube was decoded with a lock-in amplifier (SR830; Stanford Research Systems, Sunnyvale, CA) set to detect the SHG signal at the optical chopper frequency. A Labview program was used to coordinate the motion of the translation stage by use of a motion controller

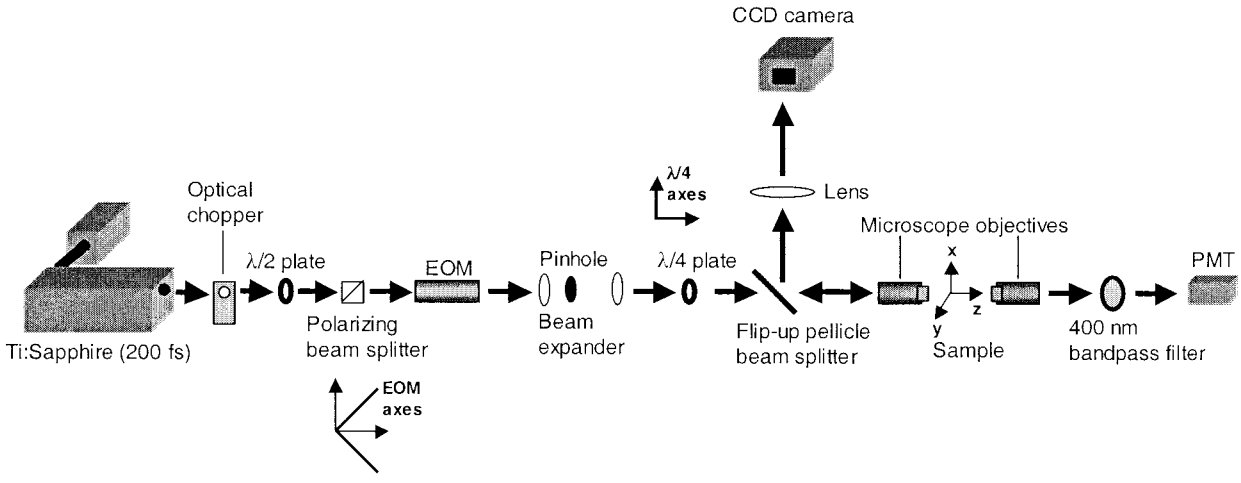

Fig. 1. Schematic diagram of the experimental setup.

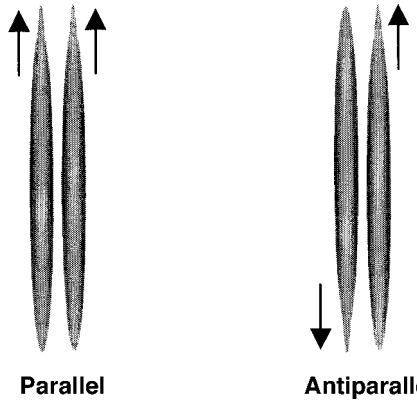

Fig. 2. Parallel (resulting in enhanced second-harmonic signal) and antiparallel (resulting in cancellation of second-harmonic signal) orientation of neighboring collagen fibrils.

(ESP300; Newport, Irvine, Calif.) and Newport 850F actuators and to acquire data from the lock-in amplifiers.

B. Sample Preparation

Rat tail tendon from 3–4-month old Sprague–Dawley rats was frozen at −20 °C until it was used. We had previously found that freezing and thawing did not affect the second-harmonic signal. Individual tendon fascicles were removed from the tendon bundles under a dissecting microscope. Typical fascicles were several centimeters long and had a diameter of only a few tenths of a millimeter. Frozen sections (4 μm) were prepared; serial slices were obtained from approximately 20 to 30 μm below the surface. The unstained frozen sections were mounted upon glass slides beneath a coverslip.

3. Theory

A. Modeling Power Generated at the Second-Harmonic Frequency in Collagen

We seek to understand the variability in a second-harmonic signal as a function of position in tendon samples and to identify the spatial scale on which it occurs. To do so, we use different microscope objectives and fill their backapertures to differing degrees to generate second harmonic images in the same sample with a wide range of numerical apertures. The second-harmonic signal generated by a focused beam in collagen depends on a number of factors: The incident laser power, the thickness of the collagen sample, the properties of the focusing, and the dispersion of light in collagen, among others, must be taken into account. The total power generated also depends strongly on the relative orientation of neighboring fibrils. Two neighboring fibrils pointing in the same direction (with respect to the orientation of the C and N termini of their component molecules) will generate second-harmonic fields that are in phase with each other and lead to enhanced SHG; two neighboring fibrils pointing in opposite directions, however, will interfere destructively, leading to reduced SHG (Fig. 2).[17] Several recent studies of both SHG and two-photon fluorescence have highlighted the importance of this effect in SHG microscopy of biological tissue. For instance, Campagnola *et al.*[2] observed cancellation of the SHG signal in tubulin structures, and this effect was also observed in styryl dye molecules attached to biological membranes.[19–21]

Dispersion in collagen leads to a difference in the indices of refraction of light with a wavelength of 800 nm (laser wavelength; index of refraction, n_1) and of light with a wavelength of 400 nm (second-harmonic wavelength; index of refraction, n_2) of the order of $\Delta n = -0.03$; the index of refraction of collagen is ~ 1.5.[22–24] As a consequence, coherence between the fundamental and the second harmonic is maintained over a distance less than $l_c = 7$ μm, which is comparable with the 4-μm thickness of the frozen sections that we use. Therefore, if all the fibrils in the interaction region are pointing the same way, the signal should be strongly enhanced. If the fibril orientation is random, such that some fibrils point in one direction and others in the opposite direction, the signal should be significantly weaker.

Here we give a simple expression for the power of the second-harmonic light generated with the assumption that all the fibrils point in one direction—this gives a maximum value for the amount of second-harmonic light that could be generated. We assume a Gaussian input laser beam focused to a diffraction-limited spot, with $1/e$ radius w_0 and Rayleigh range z_R. Using the theory described by Byer[25] and Boyd,[26] we get

$$P_{2\omega} = \frac{2|d_{\mathrm{eff}(c)}|^2}{\pi {w_0}^2} \frac{{\omega_1}^2}{{n_1}^2 n_2 c^3 \varepsilon_0} {P_{1\omega}}^2 |J(-z_f, -z_f + L_c, z_R, \Delta k_c)|^2. \quad (1)$$

In Eq. (1), ω_1 is the frequency of the incident light, $d_{\mathrm{eff}(c)}$ is the effective nonlinear susceptibility of collagen, $P_{1\omega}$ is the input laser power, $P_{2\omega}$ is the second-harmonic light power, n_1 is the index of refraction of collagen at the laser frequency and n_2 is the index of refraction at the second-harmonic frequency, c is the speed of light in air, ε_0 is the permeability of free space, and

$$J(z_f, -z_f + L_c, z_R, \Delta k_c) = \int_{-z_f}^{-z_f + L} \frac{\exp(i \Delta k_c z)}{1 + iz/z_R} \, \mathrm{d}z. \quad (2)$$

The thickness of the sample is given by L_c and the focal depth of the beam in the sample by z_f; z_R is the Rayleigh range of the focused beam, and $\Delta k_c = 2k_1 - k_2$ is the phase mismatch, where the wave vectors are defined as $k_1 = 2\pi n_1/\lambda_1$ and $k_2 = 2\pi n_2/\lambda_2$ (λ_1 and λ_2 are the wavelengths in vacuum of the laser and of the second-harmonic light, respectively).

As noted above, this calculation gives the maximum possible second-harmonic power that can be detected in a collagen sample; it assumes that the entire sample volume is occupied by collagen and that

all the fibrils are oriented in the same direction. Because rat tail tendon is approximately 60% collagen by volume,[27] the actual signal would be further reduced by ~40%.

B. Second-Harmonic Generation Signal-Strength Calibration: Using a Quartz Wave Plate

It is clear from Eqs. (1) and (2) that the second-harmonic signal in collagen depends strongly on the Rayleigh range z_R (which is directly related to focal spot radius w_0 by the expression $z_R = n_1\pi{w_0}^2/\lambda$). Therefore, even if we hold the input laser power constant, we cannot directly compare SHG signal measurements made with objective and collimating lens combinations with different numerical apertures for focusing the beam. We must obtain information about z_R for each of the numerical apertures that we use to be able to make useful comparisons. Whereas it is possible in theory to calculate the effective numerical aperture and associated Rayleigh range that will result from a given laser beam profile, spatial filter, and focusing objective, this in fact is difficult to do accurately in practice. We present a technique that uses measurements of the second-harmonic signal in quartz, which has a known second-order nonlinear susceptibility, to determine z_R directly. Using quartz to calibrate our experimental setup has the added advantage of allowing us to determine the power of the second-harmonic signal generated in collagen.

The optic axis of the quartz wave plate is in the plane of the wave plate, and the laser beam propagates normally to this plane; Fig. 3(a) illustrates this geometry. SHG in the quartz wave plate is given as a function of focal depth by[25,26]

$$P_{2\omega} = \frac{2|d_{\mathrm{eff}(q)}|^2}{\pi {w_0}^2}\frac{{\omega_1}^2}{{n_1}^2 n_2 c^3 \varepsilon_0} {P_{1\omega}}^2 |J(-z_f, -z_f + L_q, z_R, \Delta k_q)|^2, \quad (3)$$

where L_q refers to the thickness of the quartz plate, $d_{\mathrm{eff}(q)}$ is the effective second-order nonlinear susceptibility of quartz, and Δk_q is the phase mismatch in quartz. Figure 3(b) shows several examples of the theoretical depth dependence of SHG in quartz for several values of z_R. There is a unique relationship between the full width at half-maximum (FWHM) of the peaks in the signal at the two surfaces of the wave plate and z_R. Therefore we can use the quartz wave plate to directly determine z_R for different microscope objectives and collimating lenses.

Why does the second-harmonic signal peak at the surfaces of the wave plate? The peak is related to the Gouy phase shift: The phases of both the laser and the second-harmonic electric fields are shifted as they pass through the focus, but the phase of the second-harmonic polarization is shifted by twice as much as the propagating light. The fact that the second-harmonic light generated before the focus and the second-harmonic light generated after the focus are out of phase leads to cancellation of the second-harmonic light in the bulk of uniform samples, such as a quartz crystal. A large SHG signal occurs only when the beam is focused at the front or back surface of the quartz. By third-harmonic generation microscopy, the effect of the Gouy phase shift has been applied to obtaining information about the dispersion and nonlinear susceptibilities of materials at interfaces.[28,29]

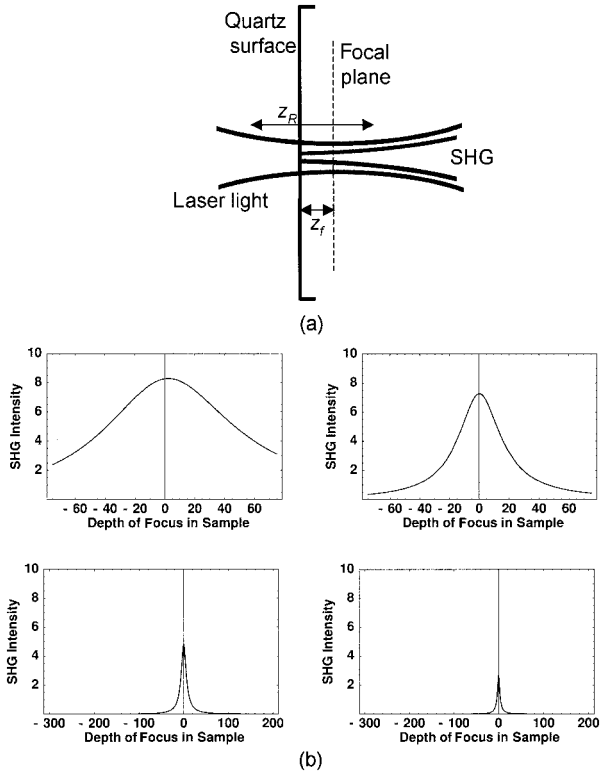

Fig. 3. (a) SHG measurement in quartz. (b) Theoretical calculation of second-harmonic signal as a function of depth of focus (depth in sample increases with increasing z) generated in a quartz wave plate ($z = 0$ is the air–quartz interface) by beams focused with different Rayleigh ranges: top left, 50 μm; top right, 15 μm; bottom left, 5 μm; bottom right, 2 μm.

The theory reflected in Eqs. (1)–(3) makes the paraxial approximation, which assumes that the polarization of the laser light is unchanged in the focus. This is not strictly true, especially when there is tight focusing (high numerical aperture). The theory [see Eq. (3)] predicts a quantitative scaling for the SHG signal as a function of the beam parameters of the focused light:

$$P_{2\omega} \propto \frac{|J(-z_{f\max}, -z_{f\max} + L_q, z_R, \Delta k_q)|^2}{{w_0}^2}. \quad (4)$$

We used the peak value of $|J|^2$ as a function of focal depth ($z_f = z_{f\max} \sim 0$). To test how well the theory applies to the measurements, we compared the peak second-harmonic signals obtained with different microscope objectives and collimating lenses. The peak signal should be related to the spot radius through relation (4). We estimated the spot radius indirectly from Rayleigh range z_R of the focused

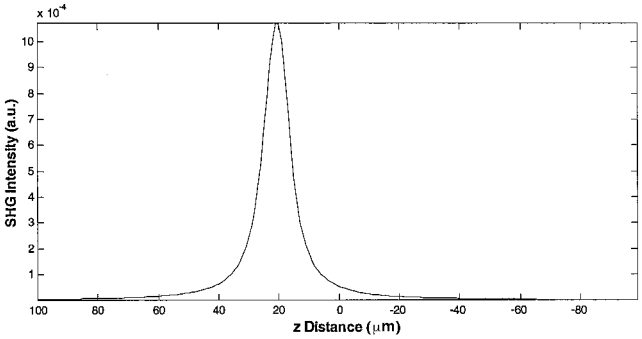

Fig. 4. Intensity of second-harmonic signal as a function of depth in quartz near the top surface (increasing z corresponds to increasing depth in the sample) for the 20× objective and a 1-μm scan resolution (arbitrary origin).

beam. Our measurements and calculations suggest that the scaling in relation (4) holds for our beam and the focusing conditions (see Subsection 4.A below). This conclusion gave us confidence that we could use the quartz signal to calibrate the setup.

By referencing the collagen signal against the quartz standard we could determine the magnitude of the elements of the nonlinear susceptibility tensor. Assuming the same laser input power and spot radius, for a given ratio of the signal in collagen V_c to the signal in quartz V_q we obtained

$$d_{\mathrm{eff}(c)}{}^2 = \frac{V_{\mathrm{collagen}}|J(z_{f\max},\ -z_f + L_q,\ z_R,\ \Delta k_q)|^2}{V_{\mathrm{quartz}}|J(-z_f,\ -z_f + L_c,\ z_R,\ \Delta k_c)|^2}\, d_{\mathrm{eff}(q)}{}^2. \tag{5}$$

The ordinary index of refraction at the laser frequency is $n_1 = 1.5383$, and the ordinary index of refraction at the second-harmonic frequency is $n_2 = 1.5577$.[30] The index of refraction in collagen is approximately 1.5. We assumed in obtaining Eq. (5) that the indices in collagen and quartz can be taken to be equal where they appear in formulas (1) and (3) but not where they appear in Eq. (2). We must take into account the difference in Δk between collagen and quartz because $|J|^2$ is highly sensitive to this difference.

C. Dependence of Second-Harmonic Generation on Polarization Angle

SHG is sensitive to the polarization of the incident laser light. In Eq. (5) above this dependence was incorporated into the effective susceptibilities of quartz and collagen, $d_{\mathrm{eff}(c)}$ and $d_{\mathrm{eff}(q)}$, respectively. If we choose a coordinate system in which the collagen fibril is oriented along the x axis and the laser beam propagates along the z axis, the second-harmonic signal will be proportional to

$$I_{\mathrm{SHG}} \propto \tfrac{1}{8}\,(3 + 20\gamma + 40\gamma^2) - \tfrac{1}{2}\,(1 + 6\gamma + 8\gamma^2)\cos(2\alpha) + \tfrac{1}{8}\,(1 + 4\gamma)\cos(4\alpha), \tag{6}$$

where α is the angle that the laser polarization makes with the x axis and γ is a parameter of the second-order nonlinear susceptibility, previously measured to be $\gamma \sim -0.65$.[11] As we use polarization modulation—the incident light's polarization is rotated from 0 to 180 deg in a sawtooth pattern at a frequency of 4 kHz—the terms that contain α are modulated at harmonics of the EOM frequency. However, we detect the signal at the chopper frequency, and thus the signal that we measure is proportional only to the first term in relation (6). From relation (6) it can be shown that, in this case, the element of the second-order nonlinear susceptibility tensor $d_{XXX(c)}$ is related to $d_{\mathrm{eff}(c)}$ by

$$d_{XXX(c)}{}^2 = 1.05 d_{\mathrm{eff}(c)}{}^2. \tag{7}$$

It is also possible to show that $d_{XYY(c)} = d_{YXY(c)} = d_{YYX(c)} = 0.68\, d_{XXX(c)}$.

In quartz (we chose the z axis to be the optic axis and the y axis to be the laser propagation direction), the polarization dependence of the second-harmonic signal is given by

$$I_{\mathrm{SHG}} \propto \tfrac{3}{8} + \tfrac{1}{2}\cos(2\pi\alpha) + \tfrac{1}{8}\cos(4\pi\alpha), \tag{8}$$

where, again, α is the angle that the laser polarization makes with the x axis. Because we detect the signal at the chopper frequency, the measured signal is again proportional only to the first term in relation (8). It can be shown that

$$d_{XXX}{}^2 = 2.67 d_{\mathrm{eff}(q)}{}^2, \tag{9}$$

where $d_{XXX(q)} = 0.40$ pm/V.[26]

4. Results and Discussion

A. Calibration

We measured the second-harmonic signal in a quartz wave plate to establish it as a reference standard. Using the measurements in quartz and applying relation (5), we could determine a minimum value for the second-order nonlinear susceptibility in collagen. As discussed in Section 3 above, we needed to measure more than the peak second-harmonic signal in quartz; we had also to measure Rayleigh range z_R. For each microscope objective and collimating lens combination we performed 20 depth scans (1-μm resolution) over a 100–200-μm axial range (depending on the objective) near the front surface of the quartz. The scans were spaced 1 μm apart in the transverse direction. We averaged the results to obtain curves of the second-harmonic signal as a function of depth, such as the example plotted in Fig. 4. Because spherical aberration at the quartz interface affects the peak SHG signal when the focus is at the back surface of the quartz wave plate, we used only results obtained from the front surface. All these results were obtained with an incident average laser power of 15.0 mW (measured before the microscope objective). We are interested in the magnitude (maximum signal) and shape FWHM of the peak in SHG signal that occurs at the front surface of the quartz wave plate. The results for all the microscope objec-

Table 2. SHG in a Quartz Wave Plate for Several Objective and Collimating Lens Combinations

Microscope Objective	f-Number of Collimating Lens (mm)	Peak SHG Signal (mV; 15-mW incident power)	FWHM of SHG Signal Peak (μm)
10×	100	0.19	130.1
10×	200	0.54	35.0
20×	50	0.32	61.1
20×	100	0.54	29.6
20×	200	1.07	10.5
40×	50	0.89	16.5
40×	100	1.26	10.0
40×	200	0.74	6.1

tive and collimating lens combinations are summarized in Table 2.

The width of the second-harmonic peak at the front surface of the quartz wave plate is related to the Rayleigh range of the focused beam. It is possible to calculate the Rayleigh range from the FWHM of the measured second-harmonic peak. The Rayleigh range is defined as $z_R \equiv n_1\pi w_0^2/\lambda$, and the focal spot's radius is related to the numerical aperture by $w_0 \approx 0.61\lambda/\text{N.A.}$ Therefore we can calculate both spot radius w_0 and the numerical aperture from the Rayleigh range. In Table 3 we list Rayleigh range z_R, focal spot radius w_0, effective numerical aperture, $|J|^2$, and $|J|^2/w_0^2$ calculated from the measured FWHM for each microscope objective (the focal length of the beam expander's collimating lens is given in parentheses beside the value of the microscope objective's magnification.

Relation (4) predicts a scaling relation for SHG as a function of w_0. In Fig. 5 we plot the ratio of the theoretical peak signal (normalized to the peak signal calculated for the 10× objective and the 100-mm collimating lens) to the measured peak signal (also normalized) versus the numerical aperture of each combination of objective and collimating lenses that we used. If the predicted scaling is satisfied, all the points plotted should fall on a line of slope 1. Figure 5 shows that there is reasonable agreement between the measured and theoretical ratios of the SHG signal from the different objectives. This holds true even for numerical apertures larger than 0.4, where the paraxial approximation used in our calculations begins to break down.

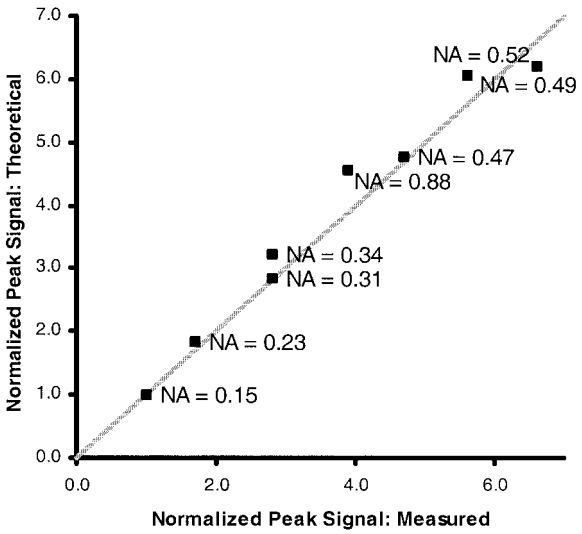

Fig. 5. Plot of the theoretically calculated peak signal (normalized to the value calculated for the 10× objective and the 100-mm collimating lens) versus the measured peak signal (normalized to the value measured for the 10× objective and the 100-mm collimating lens). Filled squares, data points; gray line (slope of 1), value expected for perfect agreement between theory and measurement.

There are several factors that can explain the discrepancies (of as much as ~20%) between theory and experiment and the fact that, in a few cases, the effective numerical aperture exceeded the nominal value. Our theory assumes a Gaussian beam; it neglects the fact that the beam incident upon the back aperture of the objective is the central maximum of the pattern produced by the spatial filter. We also do not take into account the fact that the polarization of tightly focused beams is not simply normal to the propagation direction but contains additional components. Researchers who previously investigated the qualitative effect of changing the numerical aperture on SHG microscopy[31] also noted that different group

Table 3. SHG in Quartz, Determining z_R, w_0, and $|J|^2$

Microscope Objective/Focal Length of Collimating Lens (mm)	FWHM (μm)	z_R (μm)	w_0 (μm)	N.A.	$\lvert J\rvert^2$ (μm^2)	$\lvert J\rvert^2/w_0^2$
10×/100	130.1	60.7	3.2	0.15	11.4	1.1
10×/200	35.0	15.0	1.6	0.31	8.0	3.2
20×/50	61.1	27.7	2.1	0.23	9.5	2.1
20×/100	29.6	12.5	1.4	0.34	7.5	3.6
20×/200	10.5	3.7	0.8	0.63	4.2	6.9
40×/50	16.5	6.3	1.0	0.47	5.7	5.4
40×/100	10.0	3.5	0.8	0.64	4.0	7.0
40×/200	6.1	1.9	0.6	0.88	2.6	5.1[a]

[a]Because the 100× objective (N.A., 0.7) used to collect the second-harmonic light does not actually collect all the light generated by the 40× objective (N.A., 0.9), this value has been multiplied by a correction factor of 0.61.

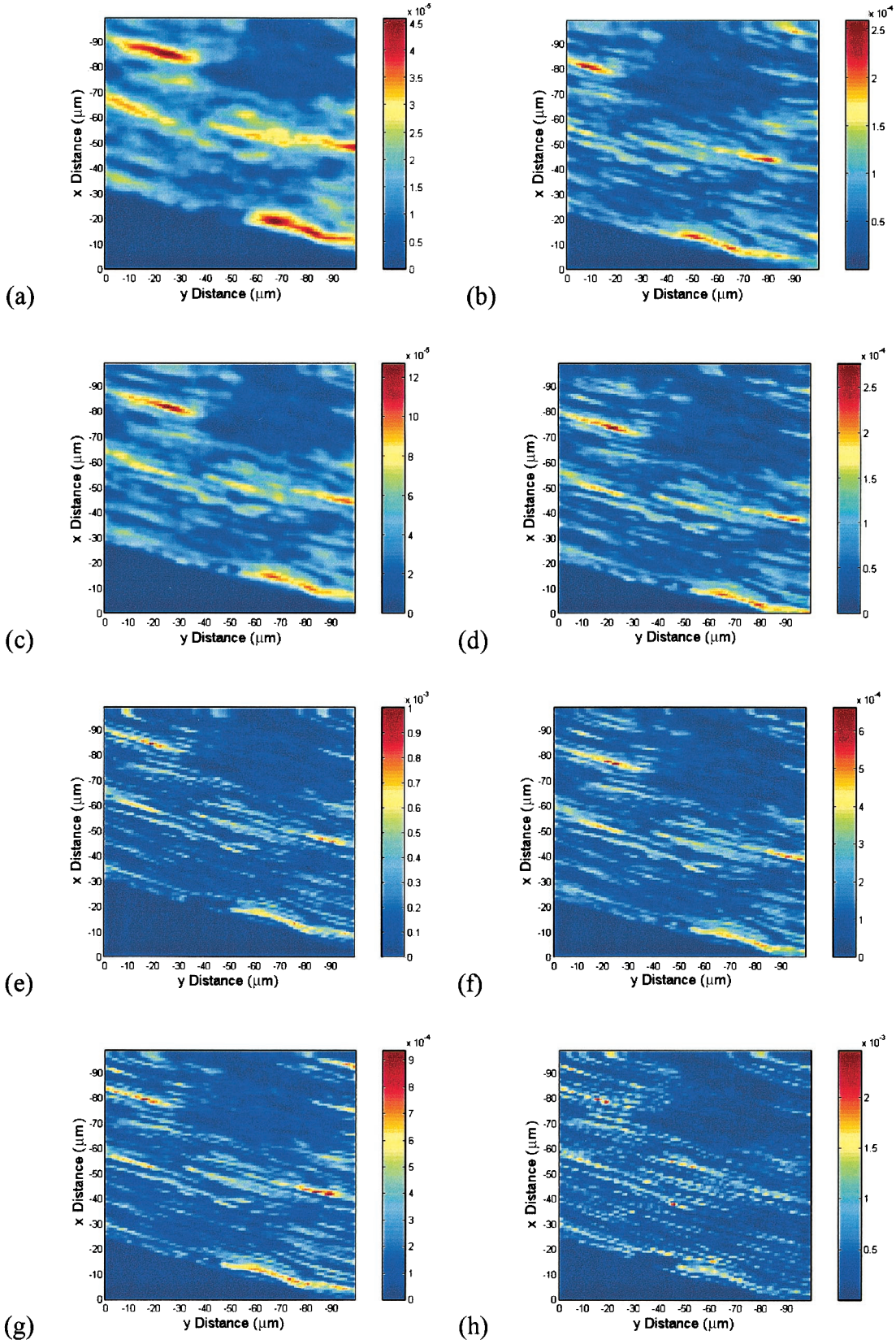

Fig. 6. Second-harmonic signal as a function of transverse position in a section of rat tail tendon obtained with a 1-μm scan resolution and (a) the 10× objective with the 100-mm collimating lens, (b) the 10× objective with the 200-mm collimating lens, (c) the 20× objective with the 50-mm collimating lens, (d) the 20× objective with the 100-mm collimating lens, (e) the 20× objective with the 200-mm collimating lens, (f) the 40× objective with the 50-mm collimating lens, (g) the 40× objective with the 100-mm collimating lens, and (h) the 40× objective with the 200-mm collimating lens. The sharp edges in the higher-resolution images are due to the finite pixel size; the data are not smoothed.

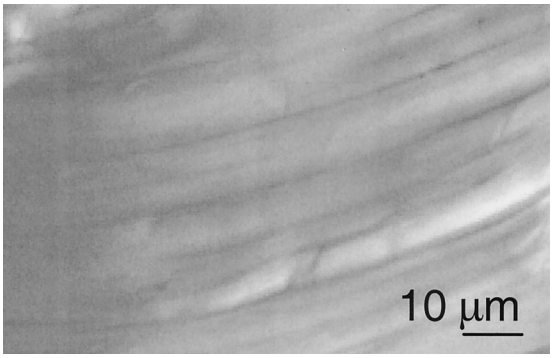

Fig. 7. Polarization microscope image of a section of rat tail tendon.

velocity dispersions in different microscope objectives may play a role in this effect.

B. Spatial Variability of the Second-Harmonic Generation Signal in Rat Tail Tendon Sections

The regional variation of collagen fibril orientation is poorly understood. Previous electron microscopy studies[27] indicated that collagen fibrils are oriented up and down in a random manner, whereas previous sum-frequency generation experiments[18] suggested that there are regions of fibrils oriented in the same direction. But on what scale do fluctuations in the orientation occur? Freund *et al.*[18] concluded that these fluctuation occur over regions less than 5 μm in width, the resolution of their crossed-beam sum frequency generation experiment. If the fluctuations occur over regions of ~1 μm in diameter, they will be consistent with the results of electron microscopy (several larger fibrils randomly oriented parallel to one another would have a diameter of ~1 μm). The use of ultrashort pulse lasers allows SHG microscopy measurements to be made at higher resolution without damaging the sample.

For each microscope objective and collimating lens combination we measured the second-harmonic signal in a 100 μm × 100 μm region of a frozen section of rat tail tendon, using a 1-μm scan resolution. The resultant images are shown in Fig. 6; we applied no smoothing, better to illustrate the difference in resolution. The intensity measurements obtained clearly fluctuate over a broad range between the noise floor and the maximum signal in all the images. There is also a large variation in SHG signal among the images (signal strength generally increases with tighter focusing and higher resolution); note that each image in Fig. 6 uses a different color scale.

There are two possible reasons for the large variation in signal strength one can see in Fig. 6. One is simply that there are narrow, localized bands of much higher collagen density. However, no studies in the literature that we are aware of report on any significant variation in density with position in rat tail tendon (refer, for instance, to Ref. 32). Furthermore, under polarization microscopy (which is sensitive to collagen density but not to fibril orientation), narrow bands of high collagen density were not observed. We would expect narrow, bright lines corresponding to increased birefringence in such images, but none were seen (Fig. 7 gives an example of a polarization microscope image of a section of rat tail tendon). There are some variations in brightness in the polarization microscope image; however, these variations are on a much longer spatial scale and can probably be explained by variations in the density or thickness of the sample. A more likely explanation for the presence of narrow bands of strong signal, then, is the presence of regions where neighboring fibrils are oriented parallel (instead of antiparallel) to each other. This parallel orientation can lead to coherent enhancement of the SHG signal, resulting in narrow regions where the signal is stronger than in areas where neighboring fibrils are oriented antiparallel.

We can investigate this effect in a more quantitative way by comparing the distribution of the second-harmonic signal strength observed by use of different numerical apertures. Figure 8(a) is a log–log plot of the number of points with a given SHG signal strength versus the signal strength. Clearly, signal strength increases with decreasing focal spot diameter, but this is so mainly because the tighter focusing allowed by a higher numerical aperture increases the intensity of the laser light in the focus. We normalized the SHG data for each image in Fig. 6 by removing the $1/w_0^2$ scaling expected from relation (4). This normalization should serve to reveal effects associated with averaging over a finite focal spot size. In Fig. 8(b) we show a log–log plot of the number of points with normalized SHG signal strength versus the normalized signal strength for each microscope objective and collimating lens used. The focal spot diameter measured with the quartz wave-plate ($2w_0$) is given as a reference for each curve. Only use of the highest numerical aperture (smallest focal spot diameter) led to a large number of points with a significantly stronger normalized signal than was observed with the other numerical apertures. This result suggests that the polarity of neighboring fibrils becomes nonrandom only on scales comparable to or smaller than the ~1.1-μm focal spot diameter formed by the highest numerical aperture objective. The small size of these regions suggests that several coaligned large-diameter fibrils (~0.5 μm) could be responsible for the enhanced SHG signal. Such coorientation of larger fibrils would be consistent both with the generally random up-and-down fibril orientation observed in electron microscopy studies and with the observations of Freund *et al.*[18]

C. Lower Bound on the Nonlinear Susceptibility of Collagen

As discussed above, we can use the SHG signal strength in the quartz wave plate to calibrate the experimental setup; this allows us to determine the second-order nonlinear susceptibility in a given sample. In rat tail tendon collagen, the degree of parallel and antiparallel orientation of neighboring fibrils

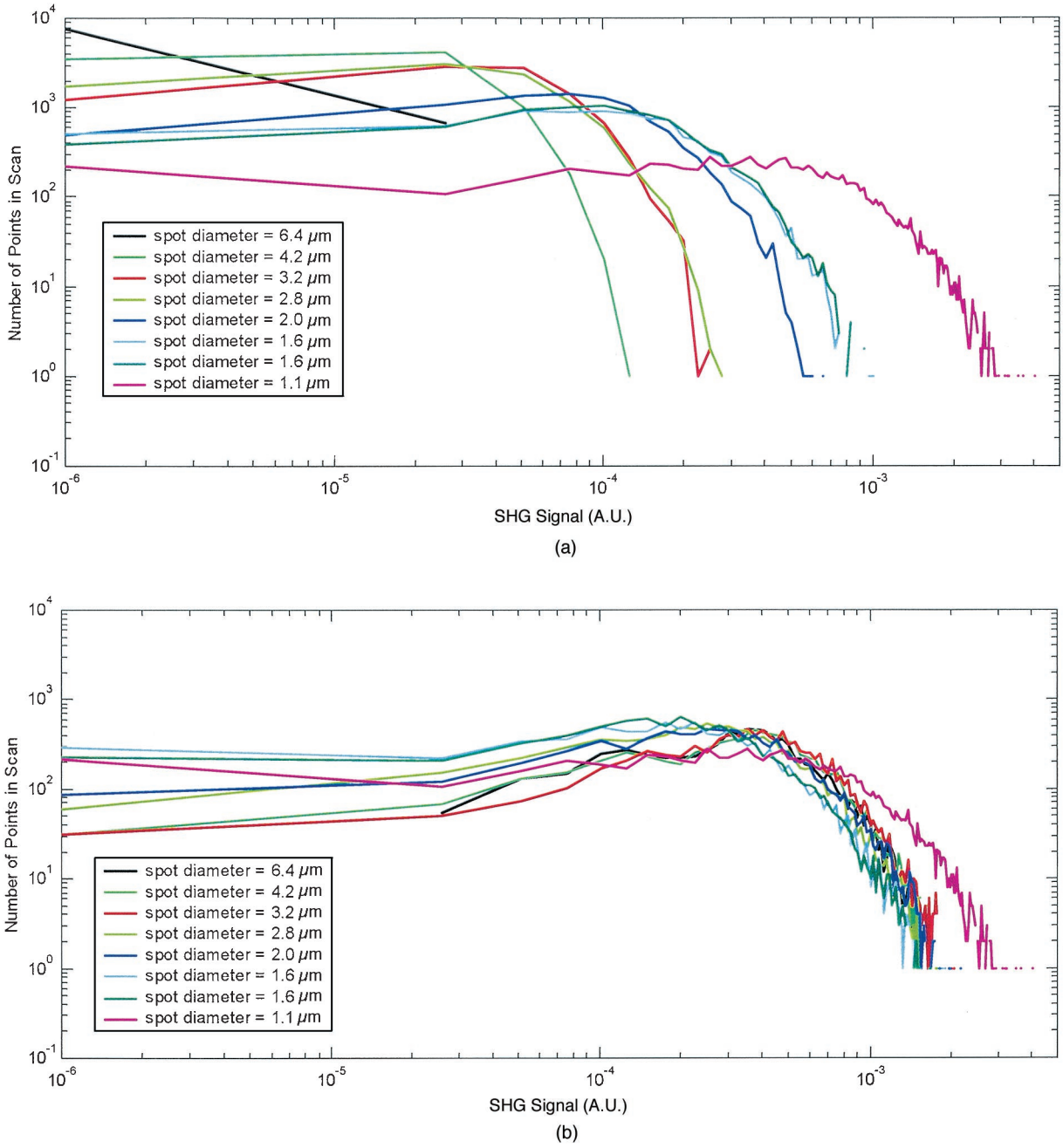

Fig. 8. Log–log plot of the frequency of occurrence versus second-harmonic signal intensity for the images shown in Fig. 5. The data are plotted by use of a different color for each of the objective–collimating lens combinations. The focal spot diameter calculated from the measurements in the quartz wave plate is given for each objective (refer to Table 3). In (a) the intensity data are not scaled (only the signal strength for a N.A. of 0.9, where significant undercollection of the signal occurs, has been corrected); in (b) the intensity data were scaled to compensate for the fact that intensity increases in inverse proportion to the square of the focal spot diameter. The intensity data were divided into 200 equally sized bins spanning the range 10^{-6}–5×10^{-3} mV.

can strongly influence the strength of the detected signal. We can calculate only a lower bound on the second-order nonlinear susceptibility. To obtain this lower bound we must first measure the SHG signal in both quartz and collagen. In quartz, for each microscope objective and collimating lens combination we used the peak signal when the laser beam was focused on the front surface of the wave plate (see above). As noted above, we also measured the second-harmonic signal in a 100 μm × 100 μm region of a frozen section of rat tail tendon, using a 1-μm scan resolution (Fig. 6). We used the peak signal in each image to calculate the lower bound on the nonlinear susceptibility.

Using Eqs. (5), (7), and (9) and taking into account the fact that tendon is only ~60% collagen,[27] we calculated d_{XXX}, $d_{XYY} = d_{YXY} = d_{YYX}$, where we let X represent the fibril axis and Y the normal to the fibril

Table 4. Lower Bound on the *d*-Tensor in Collagen

Microscope Objective/Focal Length of Collimating Lens (mm)	N.A.	Peak Signal in Collagen (mV)	Peak Signal in Quartz (mV)	d_{XXX} (pm/V)	$d_{XYY} = d_{YXY} = d_{YYX}$ (pm/V)
10×/100	0.15	0.05	0.19	0.13	0.09
10×/200	0.31	0.26	0.54	0.15	0.10
20×/50	0.23	0.13	0.32	0.14	0.10
20×/100	0.34	0.28	0.54	0.16	0.11
20×/200	0.63	1.00	1.07	0.19	0.13
40×/50	0.47	0.66	0.89	0.18	0.12
40×/100	0.64	0.94	1.26	0.17	0.12
40×/200	0.88	2.50	0.74	0.40	0.28

and the beam propagation direction. The results are summarized in Table 4. We obtained values for d_{XXX} of 0.13–0.40 pm/V. The highest value of d_{XXX} = 0.40 pm/V was obtained for the highest numerical aperture that we used (=0.9). This result again suggests that, for focal spot diameters greater than 1.1 μm, significant averaging is occurring over regions with strong SHG signal and regions with weaker SHG signal. For a focal spot diameter of less than 1.1 μm, collagen fibrils in the focus may have predominantly one polarity or another, leading to coherent SHG and thus to an enhanced signal. It should be noted that the peak signal in a single 100 μm × 100 μm image of part of a tendon section typically occurs only at a few isolated points.

5. Conclusion

We have presented a technique that uses second-harmonic generation in a quartz plate to determine the spot diameter and the Rayleigh range of an intense, tightly focused beam. We have used this technique to study the variability of the second-harmonic signal in rat tail tendon samples. Our measurements indicate that the variation in second-harmonic signal strength with transverse position is likely due to the degree of parallel and antiparallel orientation of neighboring fibrils; parallel fibrils contribute coherently to the second-harmonic signal, whereas the second-harmonic light from antiparallel fibrils interferes destructively. Regions where collagen fibrils are parallel are probably of the order of or less than 1 μm in diameter. The small size of these regions may explain why earlier SHG and sum-frequency generation experiments indicated some degree of parallel orientation of collagen fibrils, whereas electron microscopy[27] experiments suggested random parallel and antiparallel orientation of the fibrils. We were also able to place a lower bound on the magnitude of the second-order nonlinear susceptibility in collagen: $d_{XXX} > 0.4$ pm/V ($d_{XYY} = d_{YXY} = d_{YYX} = 0.7\ d_{XXX}$).

This research was supported by grants 1 R01 EB 00337-02 from the National Institutes of Health and DE-FG03-98ER62576 from the Center of Excellence for Laser Applications in Medicine, U.S. Department of Energy. This research was performed under the auspices of the U.S. Department of Energy at Lawrence Livermore National Laboratory under contract W-7405-ENG-48.

References

1. P. J. Campagnola, H. A. Clark, W. A. Mohler, A. Lewis, and L. M. Loew, "Second-harmonic imaging microscopy of living cells," J. Biomed. Opt. **6,** 277–286 (2001).
2. P. J. Campagnola, A. C. Millard, M. Terasaki, P. E. Hoppe, C. J. Malone, and W. A. Mohler, "Three-dimensional high-resolution second-harmonic generation imaging of endogenous structural proteins in biological tissues," Biophys. J. **81,** 493–508 (2002).
3. P.-C. Cheng, C.-K. Sun, B. L. Lin, F.-J. Kao, and S.-W. Chu, "Biological multi-modality nonlinear spectromicroscopy: multiphoton fluorescence, second- and third-harmonic generation," Scanning **23,** 109–110 (2001), http://www.scanning.org.
4. Y. Guo, P. P. Ho, A. Tirksliunas, F. Lui, and R. R. Alfano, "Optical harmonic generation from animal tissues by the use of picosecond and femtosecond laser pulses," Appl. Opt. **35,** 6810–6813 (1996).
5. Y. Guo, P. P. Ho, H. Savage, D. Harris, P. Sacks, S. Schantz, F. Liu, N. Zhadin, and R. R. Alfano, "Second-harmonic tomography of tissue," Opt. Lett. **22,** 1323–1325 (1997).
6. B.-M. Kim, J. Eichler, and L. B. Da Silva, "Frequency doubling of ultrashort laser pulses in biological tissues," Appl. Opt. **38,** 7145–7150 (1999).
7. B.-M. Kim, J. Eichler, K. M. Reiser, A. M. Rubenchik, and L. B. Da Silva, "Collagen structure and nonlinear susceptibility: effect of heat, glycation, and enzymatic cleavage on second harmonic signal intensity," Lasers Surg. Med. **27,** 329–335 (2000).
8. K. König, "Multiphoton microscopy in life sciences," J. Microsc. **200,** 83–104 (2000).
9. J. Squier and M. Müller, "High resolution nonlinear microscopy: a review of sources and methods for achieving optimal imaging," Rev. Sci. Instrum. **72,** 2855–2867 (2001).
10. P. Stoller, B.-M. Kim, K. M. Reiser, A. M. Rubenchik, and L. B. Da Silva, "Polarization dependent optical second harmonic imaging of rat-tail tendon," J. Biomed. Opt. **7,** 205–214 (2002).
11. P. Stoller, K. M. Reiser, P. M. Celliers, and A. M. Rubenchik, "Polarization-modulated second harmonic generation in collagen," Biophys. J. **82,** 3330–3342 (2002).
12. R. M. Williams, W. R. Zipfel, and W. W. Webb, "Multiphoton microscopy in biological research," Curr. Opin. Chem. Biol. **5,** 603–608 (2001).
13. A. Zoumi, A. Yeh, and B. J. Tromberg, "Imaging cells and extracellular matrix *in vivo* by using second-harmonic generation and two-photon excited fluorescence," Proc. Natl. Acad. Sci. USA **99,** 11014–11019 (2002).

14. S. Fine and W. P. Hansen, "Optical second harmonic generation in biological tissues," Appl. Opt. **10,** 2350–2353 (1971).
15. V. Hovanessian and A. Lalayan, in "Second harmonic generation in biofiber-containing tissue," *Proceedings of the International Conference on Lasers 1996*, V. J. Corcoran and T. A. Goldman, eds. (STS, McClean, Va., 1997), pp. 107–109.
16. S. Roth and I. Freund, "Optical second-harmonic scattering in rat-tail tendon," Biopolymers **20,** 1271–1290 (1981).
17. I. Freund and M. Deutsch, "Macroscopic polarity of connective tissue is due to discrete polar structures," Biopolymers **25,** 601–606 (1986).
18. I. Freund, M. Deutsch, and A. Sprecher, "Connective tissue polarity: optical second-harmonic microscopy, crossed-beam summation, and small-angle scattering in rat-tail tendon," Biophys. J. **50,** 693–712 (1986).
19. P. J. Campagnola, M. Wei, A. Lewis, and L. M. Loew, "High-resolution nonlinear optical imaging of live cells by second harmonic generation," Biophys. J. **77,** 3341–3349 (1999).
20. L. Moreaux, O. Sandre, and J. Mertz, "Membrane imaging by second-harmonic generation microscopy," J. Opt. Soc. Am. B **17,** 1685–1694 (2000).
21. L. Moreaux, O. Sandre, S. Charpak, M. Blanchard-Desce, and J. Mertz, "Coherent scattering in multi-harmonic light microscopy," Biophys. J. **80,** 1568–1574 (2001).
22. F. P. Bolin, L. E. Preuss, R. C. Taylor, and R. J. Ference, "Refractive index of some mammalian tissues using a fiber optic cladding method," Appl. Opt. **28,** 2297–2303 (1989).
23. D. T. Poh, "Examination of refractive index of human epidermis *in-vitro* and *in-vivo*," in *Proceedings of the International Conference on Lasers '96*, V. J. Corcoran and T. A. Goldman, eds. (STS, McLean, Va., 1997), pp. 118–125.
24. D. J. Maitland, "Dynamic measurements of tissue birefringence: theory and experiments," Ph.D. dissertation (Northwestern University, Evanston, Ill., 1995).
25. R. G. Byer, "Parametric oscillators and nonlinear materials," in *Nonlinear Optics*, P. G. Harper and B. S. Wherrett, eds. (Academic, London, 1977), pp. 47–160.
26. R. W. Boyd, *Nonlinear Optics* (Academic, San Diego, Calif., 1992).
27. D. A. D. Parry and A. S. Craig, "Quantitative electron microscope observations of the collagen fibrils in rat-tail tendon," Biopolymers **16,** 1015–1031 (1977).
28. Y. Barad, H. Eisenberg, M. Horowitz, and Y. Silberberg, "Nonlinear scanning laser microscopy by third harmonic generation," Appl. Phys. Lett. **70,** 922–924 (1997).
29. J. M. Schins, G. J. Brakenhoff, and M. Müller, "Characterizing layered structures with third-harmonic generation microscopy," GIT Imag. Microsc. **1,** 44–46 (2002).
30. G. Ghosh, "Dispersion-equation coefficients for the refractive index and birefringence of calcite and quartz crystals," Opt. Commun. **163,** 95–102 (1999).
31. R. Gauderon, P. B. Lukins, and C. J. R. Sheppard, "Optimization of second-harmonic generation microscopy," Micron **32,** 691–700 (2001).
32. E. Baer, J. J. Cassidy, and A. Hiltner, "Hierarchical structure of collagen and its relationship to the physical properties of tendon," in *Collagen: Biochemistry and Biomechanics*, M. E. Nimni, ed. (CRC, Boca Raton, Fla., 1988), Vol. 2, pp. 177–199.